Available online at www.sciencedirect.com
ScienceDirect
Catalysis Today 128 (2007) 251–257
CATALYSIS TODAY
www.elsevier.com/locate/cattod

Tuning the selectivity of MoO_x supported catalysts for cyclohexane photo oxidehydrogenation

P. Ciambelli [a], D. Sannino [a,*], V. Palma [a], V. Vaiano [a], P. Eloy [b], F. Dury [b], E.M. Gaigneaux [b]

[a] *Dipartimento di Ingegneria Chimica e Alimentare, Università di Salerno, 84084 Fisciano (SA), Italy*
[b] *Unité de Catalyse et Chimie des Matériaux Divisés, Université catholique de Louvain, B-1348 Louvain-la-Neuve, Belgium*

Available online 18 September 2007

Abstract

The photocatalytic properties of sulphated MoO_x/γ-Al_2O_3 catalysts in cyclohexane oxidative dehydrogenation have been determined in a two-dimensional fluidized bed photoreactor and compared to those of sulphated MoO_x/TiO_2 catalysts. Photocatalytic tests on MoO_x/γ-Al_2O_3 at 8 wt% MoO_3 and various sulphate contents showed the selective (100%) formation of cyclohexene, without production of benzene, as instead found with MoO_x/TiO_2. These results show that the selectivity of photocatalytic cyclohexane oxydehydrogenation is dramatically influenced by the catalyst support.

Maximum cyclohexane conversion and cyclohexene yield of 11% were obtained for SO_4 content of 2.6 wt% at 120 °C. Physico-chemical characterisation of catalysts indicates the presence of both octahedral polymolybdate and sulphate species on alumina surface, as previously found for titania. Increasing sulphate load, thermogravimetry evidenced the presence of up to three sulphate species at different thermal stability. The lower activity observed at high sulphate content is likely due to polymolybdate decoration by sulphates.

Keywords: Photocatalytic cyclohexane oxidative dehydrogenation; Fluidized bed photoreactor; Sulphate

1. Introduction

The interest to investigate photocatalytic processes for synthetic purposes is recently strongly increasing: oxofunctionalization of hydrocarbons by O_2 in liquid phase is a typical example [1]. A general requirement for oxidative catalysis addressed to this goal is a very effective control of process selectivity. In liquid-phase photooxidation of cyclohexane on TiO_2, the role of solvent is critical in affecting both selectivity and products distribution through competitive adsorption effects [2]. Cyclohexane–oxygen photocatalytic reactions result in high selectivity to cyclohexanone [3], higher in neat cyclohexane when photolysis is prevented [4]. We found that completely different products such as cyclohexene or benzene are selectively obtained through gas phase oxidative dehydrogenation of cyclohexane on TiO_2 supported MoO_x at low temperature, under UV illumination in a fixed [5] or, better [6,7] in a fluidized bed reactor. Selectivity to benzene grows with the sulphate content of the support [8], whereas selectivity on unsulphated or sulphated titania is 100% to carbon dioxide [8,9]. In the present study the photoactivity of MoO_x/γ-Al_2O_3 catalysts at various sulphation degrees for cyclohexane oxidative dehydrogenation reaction has been investigated in a two-dimensional fluidized bed photoreactor.

2. Experimental

γ-Al_2O_3 (Puralox SBA 150, SASOL, 144 m^2/g) was wet impregnated with an aqueous solution of ammonium heptamolybdate $(NH_4)_6Mo_7O_{24}{\cdot}4H_2O$. Typical conditions were: 18 g of support, 2.0 L of an 7×10^{-4} M ammonium heptamolybdate solution. Powder samples were dried at 120 °C for 12 h and calcined in air with a heating rate of 10 °C/min up to 500 °C, then kept at this temperature for 3 h. All calcined catalysts have 8 wt% MoO_3 (8Mo) as nominal loading. A second wet impregnation of 8Mo with an aqueous solution of ammonium sulphate was performed, employing 14 g of 8Mo, 2.0 L of ammonium sulphate solutions, with

* Corresponding author. Tel.: +39 089964147; fax: +39 089964057.
E-mail address: dsannino@unisa.it (D. Sannino).

0920-5861/$ – see front matter © 2007 Elsevier B.V. All rights reserved.
doi:10.1016/j.cattod.2007.07.006

concentration ranging between 2.2×10^{-3} and 6.8×10^{-3} M. Powder samples were then dried at 120 °C for 12 h and calcined in air, heated up to 300 °C with a heating rate of 10 °C/min, then isotherm for 3 h. For comparison two titania supported catalysts were prepared by incipient wet impregnation of anatase phase titania (DT2), containing 2.4 wt% of SO_4 (DT51, Rhone Poulenc, 71 m^2/g) with aqueous solution of ammonium heptamolybdate, in order to obtain 5MoDT2 and 8MoDT2 catalysts after drying and calcination in air at 400 °C for 3 h.

Thermogravimetric analysis (TG-DTG-MS) of powder samples was carried out in air flow with a thermoanalyzer (Q500, TA Instruments), on-line connected with a quadrupole mass spectrometer (Quadstar 422, Pfeiffer Vacuum) in the range 20–850 °C at heating rate of 10 °C/min. Specific surface area of calcined samples, pretreated at 180 °C for 2 h in He flow (99.9990%), was obtained by N_2 adsorption isotherm at −196 °C with a Costech Sorptometer 1040.

XPS analyses were performed with a Kratos Axis Ultra spectrometer (Kratos Analytical – Manchester – UK) equipped with a monochromatised aluminium X-ray source (powered at 10 mA and 15 kV). The sample powders were pressed into small stainless steel troughs mounted on a multi specimen holder. The pressure in the analysis chamber was around 10^{-6} Pa. The angle between the normal to the sample surface and the lens axis was 0°. The pass energy was set at 40 eV. In these conditions, the energy resolution gives a full width at half maximum (FWHM) of the Ag $3d_{5/2}$ peak of about 1.0 eV. Charge stabilisation was achieved by using an electron source mounted co-axially to the electrostatic lens column and a charge balance plate used to reflect electrons back towards the sample. The magnetic field of the immersion lens placed below the sample acts as a guide path for the low energy electrons returning to the sample. The electron source was operated at 1.8 A filament current and a bias of −1.1 eV. The charge balance plate was set at −2.8 V. The Kratos device leads to a perfectly neutral sample surface, and, as a consequence, the photoelectron peaks obtained appear much narrower than those obtained with the typical flood gun technology. The following sequence of spectra was recorded: survey spectrum, C 1s, O 1s, Al 2p, S 2p, Mo 3d and C 1s again to check the stability of charge compensation in function of time and the absence of degradation of the sample during the analyses. The binding energies were calculated with respect to the C–(C,H) component of the C 1s peak fixed at 284.8 eV. The spectra were decomposed with the CasaXPS program (Casa Software Ltd., UK) with a Gaussian/Lorentzian (70/30) product function and after subtraction of a linear baseline (the application of such type of baseline is recommended by the manufacturer as it is the most suitable with the shape of the machine workfunction). Although Mo $3d_{3/2}$ and Mo $3d_{5/2}$ peaks overlap S 2s peak, it was taken into account that the theoretical distance between Mo $3d_{3/2}$ and Mo $3d_{5/2}$ peaks is 3.13 eV and the area ratio is 2/3. Also, thanks to the samples without Mo, constraints for the position and the width of S 2s peaks were determined and used for subtracting the S 2s contributions from each Mo peaks. Molar fractions were calculated using peak areas normalised on the basis of acquisition parameters, sensitivity factors provided by the manufacturer and the transmission function.

Laser Raman spectra of powder samples were obtained in air with a Dispersive MicroRaman (Invia, Renishaw), equipped with 785 nm diode-laser, in the range of 100–2500 cm^{-1} Raman shift.

UV–vis reflectance spectra of powder bare catalysts were recorded by a Perkin-Elmer spectrometer Lambda 35 using a RSA-PE-20 reflectance spectroscopy accessory (Labsphere Inc., North Sutton, NH). All spectra were obtained using an 8° sample positioning holder, giving total reflectance relative to a calibrated standard SRS-010-99 (Labsphere Inc., North Sutton, NH). The reflectance data were reported as the $F(R_\infty)$ value from Kubelka–Munk theory versus the wavelength [10]. Equivalent band gap determinations were made, assuming that the dispersed MoO_x phase behaves in light absorption in a way similar to a direct gap semiconductor, by plotting $[F(R_\infty) \times h\nu]^2$ versus $h\nu$ (eV) and calculating the x intercept of a line passing through $0.5 < F(R_\infty) < 0.8$.

Photocatalytic tests were carried out feeding 830 (stp)cm^3/min N_2 stream containing 1000 ppm cyclohexane, 1500 ppm oxygen and 1600 ppm water. Cyclohexane and water were vaporised by two temperature controlled saturators. The gas flow rates were measured and adjusted by mass flow controllers (Brooks Instrument). The reactor inlet or outlet gases were fed to an on-line quadrupole mass detector (MD800, Thermo-Finnigan) and a continuous CO–CO_2 NDIR analyser (Uras 10, Hartmann & Braun).

The fluidized bed reactor [7] has 40 mm × 10 mm cross section, 2 mm thick, and 230 mm height pyrex-glass walls. A bronze filter (5 μm size) was used for gas feeding to provide uniform gas distribution. The reactor was illuminated by four UV light sources (EYE MERCURY LAMP, 125W) with spectrum emission centred at 365 nm, in a dark box. Following a previous investigation of the temperature effect [6,7], the reactor temperature was set and controlled at 120 °C by a PID temperature controller connected to a heating system. In order to achieve fluidization conditions, 14 g of catalyst (grain size: 25–38 μm) and 63 g of α-Al_2O_3 (Aldrich, 10 m^2/g) with Sauter average diameter of 50 μm and bulk density equal to 3970 kg/m^3 were mixed and loaded to the photoreactor. For all physical mixtures no positional fractioning of two components was observed.

Lamps were switched on after complete adsorption of cyclohexane on the catalyst surface, no reaction products were observed either during the cyclohexane dark adsorption either after that cyclohexane adsorption equilibrium was reached.

3. Results and discussion

3.1. Catalyst characterisation

The list of catalysts and their characteristics is reported in Table 1. Since on MoO_x supported alumina catalysts, a surface density of 4.5–4.6 Mo/nm^2 for developing a complete surface MoO_x monolayer was reported [11,12], a coverage degree of about 50% can be calculated for all MoO_x/γ-Al_2O_3 at 8 wt%

Table 1
Catalysts and their characteristics

Catalyst	MoO_3 (wt%)	SO_4 (wt%)	SO_4* (wt%)	Specific surface area (m^2/g)	Equivalent band gap energy (eV)
8Mo	8	0	0	144	3.4
2S	0	2.4	2.5	–	–
5S	0	4.8	3.7	–	–
7S	0	7.2	6.8	–	–
8Mo2S	8	2.4	2.6	135	3.4
8Mo5S	8	4.8	4.9	114	3.3
8Mo7S	8	7.2	7.3	111	3.2
DT2	0	2.4	2.3	71	3.3
5MoDT2	4.7	2.4	2.1	68	3.3
8MoDT2	8	2.4	2.2	63	3.2

* Evaluated by TG-MS.

MoO_3. For comparison 4MoDT2 and 8MoDT2 at 57% and 100%, respectively, of monolayer capacity of titania [13,14] have been reported.

It can be seen that the specific surface area of Mo-catalysts slightly decreases with respect to supports as the sulphate content increases. Thermogravimetric curves of 8Mo, 8Mo2S, 8Mo5S and 8Mo7S, reported in Fig. 1, show two main weight loss steps: the first up to 220 °C, the second step with onset temperature of 220 °C and offset at 550 °C and 380 °C° for 8Mo2S and for 8Mo5S or 8Mo7S, respectively, associated to water removal by MS analysis. A third complex step is due to the decomposition of surface sulphates, as indicated by *m/z* signal 64. SO_2 evolution starts from 550 °C ending at 820 °C for 8Mo2S, while downshifts between 380 and 800 °C for 8Mo5S and 8Mo7S. Total sulphate loss well agrees with the nominal sulphate content (Table 1). For sulphated γ-alumina, up to three different sulphate species, according to [15], with DTG peaks at 650, 810, 950 °C have been found (not reported). DTG curves of 8Mo2S and 2S (not reported) show a single high temperature peak, centred respectively at about 717 °C and 920 °C, resulting from sulphate decomposition. The decrease in decomposition temperature with respect to sulphated support is due to the presence of MoO_x species, as previously observed [16] for titania based catalysts. On 8Mo5S in addition to a DTG peak at about 700 °C, two overlapping peaks appear, with maximum at 540 °C and 610 °C, likely due to different sulphate species coordinated on alumina. Another DTG peak, centred at about 430 °C, appears. Similar observations can be done for 8Mo7S catalyst with DTG peaks, centred at 430 °C, 523 °C, 685 °C and 745 °C due to different kind of surface sulphates. These further species, appearing at high sulphate content but absent on all the sulphated supports, should be attributed to sulphate interacting with surface molybdate. TG losses with DTG peak at 430 °C, not present on sulphated support 2S, 5S and 7S, could be attributed to the decomposition of sulphate species interacting with surface molybdates. XPS analyses showed no other photoemissions than C 1s (C=O 289.2, C–O 286.3, C–C,H 284.8 eV), O 1s (531.4 eV), Al 2p (74.7 eV) and/or Ti, S 2p (169.5 eV) and/or Mo 3d (233 eV and 231.7 eV) for all the samples, without any significant differences in the binding energies of all the elements. The presence of carbon is due to the XPS analysis (preparation of the samples, and contaminant from the ultrahigh vacuum devices associated to the machine). Table 2 summarizes some surface atomic ratios.

Fig. 2 shows that the values of surface S/Al atomic ratios increase with SO_4 loading as expected, while it is worth to note

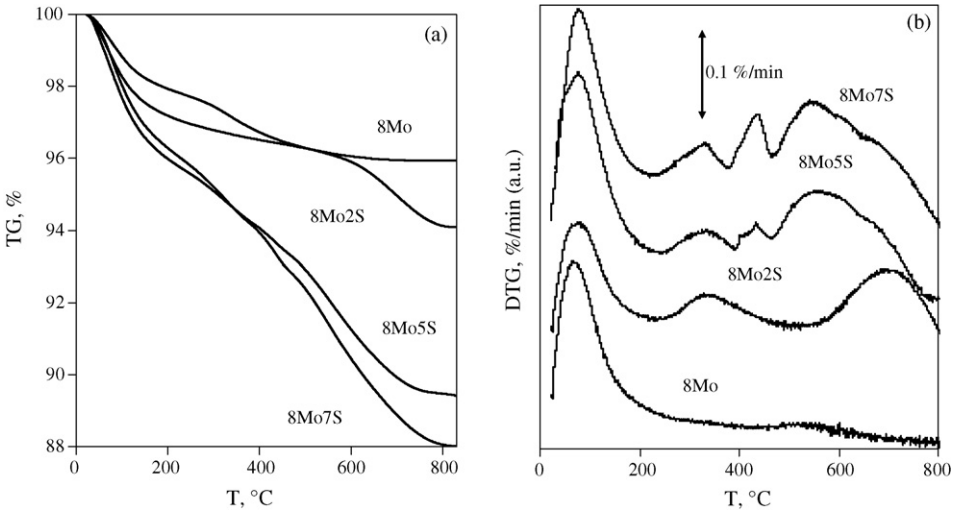

Fig. 1. TG (a) and DTG (b) curves of 8Mo, 8Mo2S, 8Mo5S and 8Mo7S catalysts.

Table 2
Surface atomic ratios

	8Mo	8Mo2S	8Mo5S	8Mo7S	2S	5S	7S
O/Al	1.56	1.64	1.59	1.66	1.60	1.66	1.61
C/Al	0.29	0.28	0.27	0.29	0.25	0.25	0.30
Mo/Al	0.044	0.043	0.037	0.026	–	–	–
S/Al	–	0.021	0.031	0.041	0.020	0.039	0.049

that surface concentration of Mo decreases with increasing the surface concentration of S, suggesting a decoration of MoO_x species by sulphate at high SO_4 contents, as also suggested by TG analysis.

The Raman spectra of all samples are reported in Fig. 3. The sulphated aluminas exhibit a band around 985 cm^{-1} whose intensity increases with the sulphate load, assigned to symmetric stretching mode ν_1 of sulphate coordinated to the surface.

The absence of bulk molybdena bands at 819 and 995 cm^{-1} [17] for all Mo-based catalysts evidences that they are monolayer or sub-monolayer catalysts. For 8Mo, bands around 950 cm^{-1} are observed. The Mo=O stretching band at 955 cm^{-1} on 8Mo, characteristic of polymolybdenyl species [12], is slightly enlarged on 8Mo2S at 956 cm^{-1} while for 8Mo5S, MoO_x and sulphate bands at 952 and 983 cm^{-1}, respectively, start to be distinguishable. At higher sulphate load (8Mo7S) three bands at 905, 951 and 984 cm^{-1} are observed. The peak at 905 cm^{-1} could be assigned to Mo=O stretching of tetrahedral species, since the peak position of ideal tetrahedral structure, like MoO_4^{2-} (aq) is at 897 cm^{-1}, rising to 910 and 928 cm^{-1} for distorted tetrahedral structures such as $(NH_4)_2Mo_2O_7$ and $(NH_4)_2Mo_2O_7$, respectively [14,19]. The presence of polymeric octahedral species and sulphate can be recognised by the peaks at 951 and 984 cm^{-1}, respectively. Since additional sulphate Mo interacting species are observed by TG-MS of both 8Mo5S and 8Mo7S, the presence of tetrahedral species could derive from the strengthening of

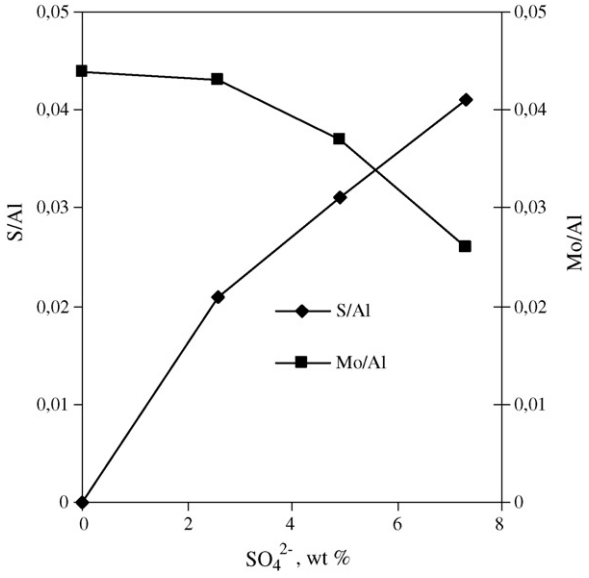

Fig. 2. S/Al and Mo/Al surface atomic ratios from XPS analysis of 8Mo, 8Mo2S, 8Mo5S and 8Mo7S as function of sulphate catalyst content.

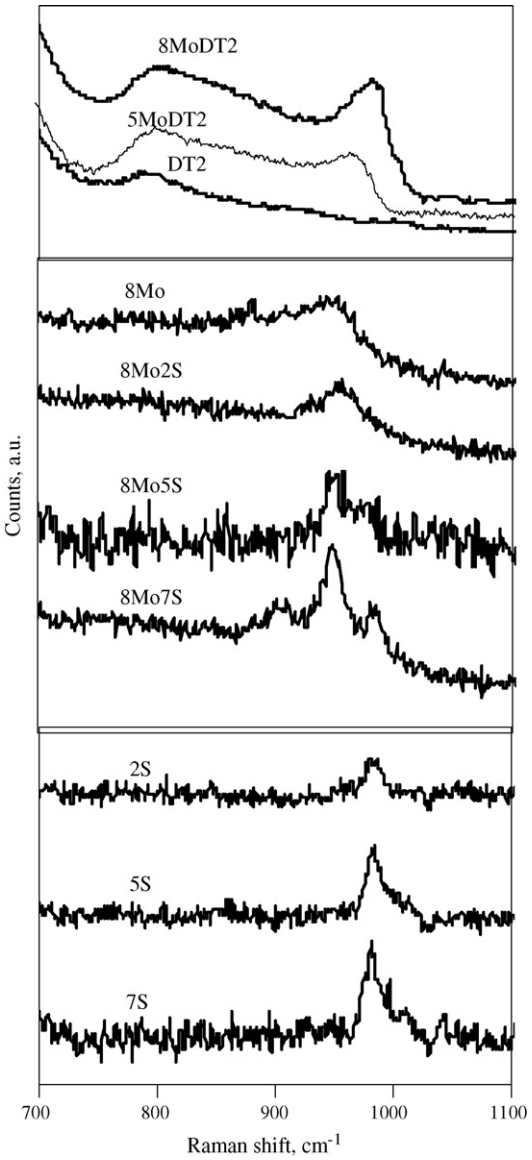

Fig. 3. Raman spectra of 2S, 5S, 7S, 8Mo2S, 8Mo5S, 8Mo7S, DT2, 5MoDT2 and 8MoDT2 catalysts.

MoO_x-sulphate interactions up to a slight decrease in the nuclearity of surface polyanions. However, Mo=O stretching of $K_3Mo_2(SO_4)_4$ 3.5 H_2O is reported to occur at 956 cm^{-1} [18], so a direct evidence for MoO_x-sulphates interaction cannot be obtained by Raman spectra. On 5MoDT2 and 8MoDT2 complex bands with maximum at about 960 and 980 cm^{-1}, respectively, indicate the presence of surface polymeric octahedral anchored species. The increase in wavenumbers with increasing Mo loading has been attributed to higher polymerisation degree of Mo species [19]. Wachs [12] reported that, in hydrated conditions, $Mo_8O_{26}^{4-}$ presents Raman Mo=O band at 960 on alumina and 963 cm^{-1} on titania. The comparison between 8Mo2S with respect to 8MoDT2 with similar MoO_x content, or with 5MoDT2 at comparable MoO_x coverage, suggests the presence of less polymerised species on alumina catalysts.

UV–vis DRS spectra (Fig. 4) show no significant absorptions related to the supports, either alumina or sulphated

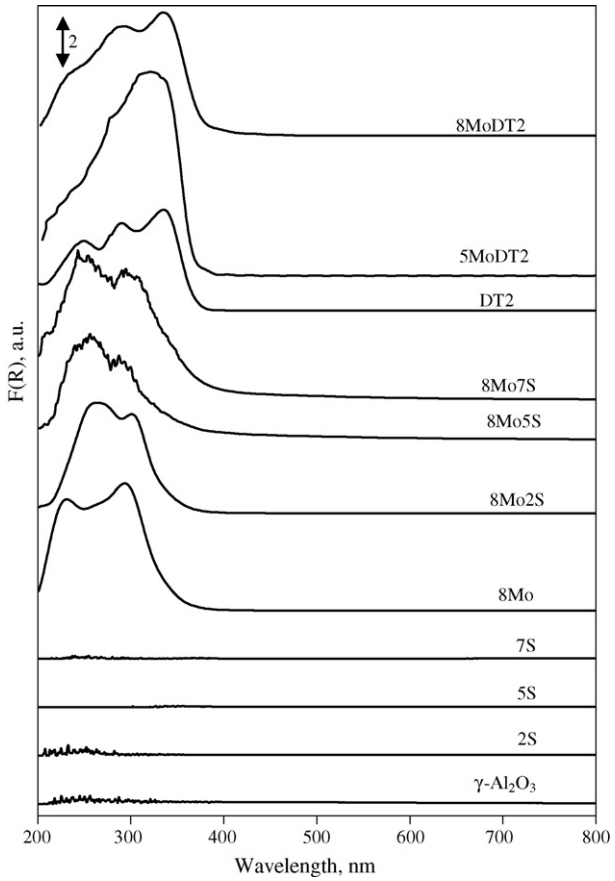

Fig. 4. UV–vis DRS spectra of γ-Al_2O_3, 2S, 5S, 7S, 8Mo2S, 8Mo5S, 8Mo7S, DT2 5MoDT2 and 8MoDT2 catalysts.

aluminas, or to the presence of MoO_3 on the catalysts, which presented main band at 360 nm [20].

On Mo/γ-alumina catalysts, composites absorption bands are due to the ligand–metal charge transfer (LMCT) $O^{2-} \rightarrow Mo^{6+}$, usually expected in the range of 200–400 nm [21,22]. From literature, the bands at 210–250 nm are commonly attributed to the tetrahedral molybdate, the bands in 230–300 nm region to octahedrally coordinated Mo^{6+} (Oh) [23], while the band at 320 nm is assigned to the Mo–O–Mo bridge bond of the octahedral coordination [20]. The contributions at around 250 and 300 nm for all Mo/γ-alumina catalysts can be attributed to the octahedrally coordinated polymolybdena species. Comparing spectra of 8Mo2S and 8Mo, it can be observed that the strong peak at 230 nm disappeared but, by increasing the sulphate load on 8Mo5S and 8Mo7S, absorption widens and the appearance of a shoulder at 210 nm could indicate the formation of tetrahedral species, according to the Raman spectra evaluations. The presence of sulphate at increasing amounts led to a red shift of the lowest energy transition absorption of molybdate, corresponding to a decrease in band gap energies, reported in Table 1. When supported on sulphated titania, Mo species absorption bands are more difficult to distinguish. However, a contribution at 310 nm on 5MoDT2 appears overimposed to support spectrum. Band gap value decreases from 5MoDT2 to 8MoDT2 but band gap energies remain similar to that observed for 8Mo5S and 8Mo7S, respectively.

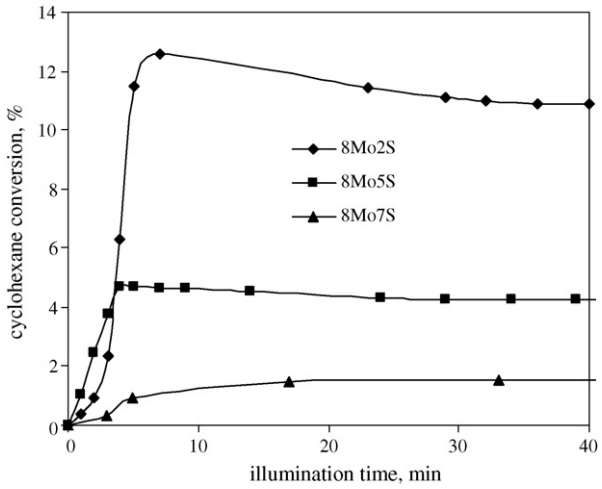

Fig. 5. Cyclohexane conversion on 8Mo2S, 8Mo5S and 8Mo7S as function of illumination time.

3.2. Catalytic tests

In order to verify that cyclohexane was converted in a heterogeneous photocatalytic process, a control test was carried out with the reactor loaded with α-Al_2O_3 alone. No conversion of cyclohexane was detected during this test, indicating the necessity of the catalyst for the observed reaction. Photocatalytic test at 120 °C was also performed mixing 14 g of 8Mo with 63 g of α-Al_2O_3. In the absence of sulphate, MoO_x/γ-Al_2O_3 catalyst (8Mo) was not active in cyclohexane conversion. In the same way, sulphated aluminas, 2S, 5S, and 7S did not show any photoactivity. By contrast, sulphated MoO_x/γ-Al_2O_3 catalysts were able to selectively convert cyclohexane to cyclohexene, without formation of benzene and CO_x as by-products (Figs. 5 and 6).

For all catalysts, cyclohexene was the only product detected in the gas phase (100% selectivity) that is formed simultaneously to cyclohexane conversion after lamp on, reaching steady state values (110 ppm, 45 ppm and 10 ppm on 8Mo2S, 8Mo5S and 8Mo7S, respectively) after about 30 min. However,

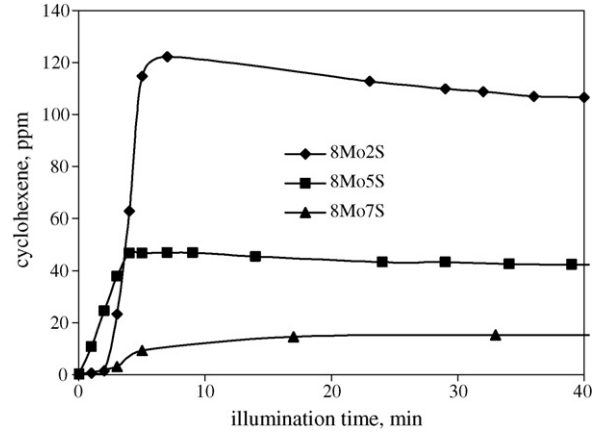

Fig. 6. Cyclohexene outlet concentration on 8Mo2S, 8Mo5S and 8Mo7S as function of illumination time.

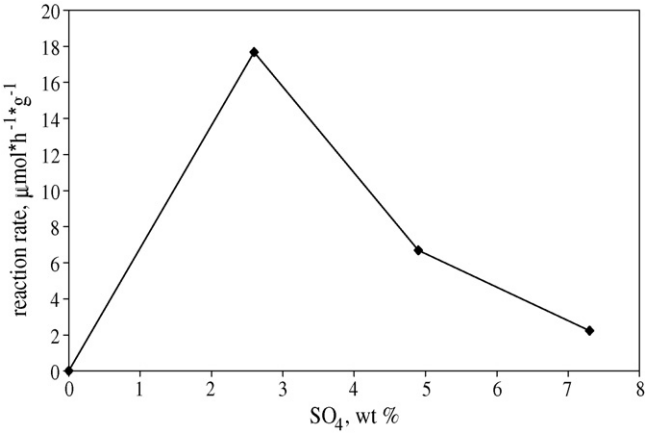

Fig. 7. Effect of sulphate content on cyclohexane reaction rate. Reaction temperature: 120 °C.

cyclohexane conversion and cyclohexene yield decreased with the sulphate content.

The results show that sulphate strongly enhances the photoactivity of MoO_x/γ-alumina catalysts.

Enhanced photoactivity has been reported for sulphated titania in 2,4-dinitroanilina decomposition, attributed to the improved transfer and separation of photogenerated electrons and holes [24]. Furthermore, the beneficial effect of additional oxidant like peroxydisulphate generating $SO_4^{\bullet -}$ and SO_4^{2-} in solar/TiO_2 mineralisation of pesticides has been evidenced by Malato et al. [25]. $SO_4^{\bullet -}$subtracts generated electrons in TiO_2 conduction band leaving a larger holes number able to give $^{\bullet}OH$. The radical anion can also react with H_2O to give $^{\bullet}OH$ or with organic compounds.

The cyclohexane reaction rate as a function of sulphate catalyst content at 120 °C is shown in Fig. 7. It has a maximum value of 18 $\mu mol \times h^{-1} \times g^{-1}$ % at 2.6 wt SO_4 loading, indicating that 8Mo2S has the higher performance in cyclohexene production.

In Table 3 the catalytic performances of 8Mo2S and sulphated MoO_x/TiO_2 catalysts are compared. While on sulphated titania very low cyclohexane conversion and 100% selectivity to CO_2 is obtained, with MoDT2 catalysts enhanced conversion and selectivity to benzene is achieved. CO_2 formation is still observed on 5MoDT2, due to the residual exposed bare sulphated titania able to mineralise cyclohexane under UV illumination, but on 8MoDT2 CO_2 is not produced anymore. On both catalysts very few amounts of cyclohexene are formed. A completely different products distribution is obtained with 8Mo2S: neither benzene nor CO_2 are formed and 100% selectivity to cyclohexene is obtained. It is worthwhile to point out that bare sulphated alumina does not show any photoactivity. Therefore the selectivity of cyclohexane photooxydehydrogenation can be effectively tuned by changing Mo load or type of support to obtain cyclohexene or benzene.

Table 3
Photocatalytic performances comparison of 8Mo2S, DT2, 5MoDT2 and 8MoDT2 catalysts

Catalyst	Cyclohexane conversion (%)	Benzene selectivity (%)	Cyclohexene selectivity (%)	Carbon dioxide selectivity (%)
8Mo2S	11	0	100	0
DT2	1.8	0	0	100
5MoDT2	18	95	0.5	4.5
8MoDT2	14	99	1	0

The different selectivity to benzene or cyclohexene, observed on the different supports, cannot be ascribed to the kind of MoO_x species or to their surface densities, since the characterisation results showed that surface polymeric octahedral MoO_x species are present on both titania and alumina, without changing the product nature also for little variations in polyanions nuclearity. On the other hand, as widely highlighted about catalytic perfomances of supported metal-oxide catalysts [26], we can affirm that specific oxide support plays a key role in determining selectivity also in gas-phase cyclohexane photocatalytic oxydehydrogenation. However, further studies are necessary to clarify the influence of metal-oxide support characteristics, on the photoreaction mechanism.

4. Conclusions

Photocatalytic oxidative dehydrogenation of cyclohexane was carried out over MoO_x/TiO_2 and MoO_x/γ-Al_2O_3 catalysts having the same MoO_3 nominal load but different sulphate content.

It was verified the possibility to produce selectively benzene or cyclohexene from the paraffin with a selectivity of 100% by using photocatalytic process. The tuning in photoreaction selectivity can be obtained by changing the support nature. Furthermore, it can be claimed that sulphate addition on MoO_x/γ-Al_2O_3 leads to a dramatic enhancing of catalyst photoactivity. An optimum in sulphate loading was found to be 2.6 wt%, for which physico-chemical characterisation indicates the presence of either octahedral polymolybdate species or surface sulphates on both alumina and titania supports. On MoO_x/γ-Al_2O_3 catalysts, decreasing in catalytic activity at higher sulphate loading could be due to MoO_x decoration by sulphates.

References

[1] A. Maldotti, A. Molinari, R. Amadelli, Chem. Rev. 102 (2002) 3811.
[2] C.B. Almquist, P. Biswas, Appl. Catal. A 214 (2001) 259.
[3] M.U. Wei, J.M. Herrmann, P. Pichat, Catal. Lett. 3 (1989) 73.
[4] P. Du, J.A. Moulijn, G. Mul, J. Catal. 238 (2006) 342.
[5] P. Ciambelli, D. Sannino, V. Palma, V. Vaiano, Catal. Today 99 (2005) 143.
[6] P. Ciambelli, D. Sannino, V. Vaiano, V. Palma, S. Vaccaro, Chem. Proceedings of the 7th World Congress of Chemical Engineering, July 10–14, Glasgow Scotland, 2005.
[7] V. Vaiano, Ph.D. thesis, University of Salerno, Italy, March 2006.
[8] P. Ciambelli, D. Sannino, V. Palma, V. Vaiano, Stud. Surf. Sci. Catal. 155 (2005) 179.
[9] H. Einaga, S. Futamura, T. Ibusuki, Appl. Catal. B 38 (2002) 215.
[10] C. Anderson, A.J. Bard, J. Phys. Chem. B 101 (1997) 2611.
[11] K. Chen, E. Iglesia, A.T. Bell, Stud. Surf. Sci. Catal. 136 (2001) 507.
[12] I. Wachs, Catal. Today 27 (1996) 437.
[13] K.Y.S. Ng, E. Gulari, J. Catal. 92 (1985) 340.
[14] D.S. Kim, Y. Kurusu, I.E. Wachs, F.D. Hardcastle, K. Segawa, J. Catal. 120 (1989) 325.

[15] M.L. Guzmán-Castillo, E. López-Salinas, J.J. Fripiat, J. Sánchez-Valente, F. Hernández-Beltrán, A. Rodríguez-Hernández, J. Navarrete-Bolaños, J. Catal. 220 (2003) 317.
[16] P. Ciambelli, M.E. Fortuna, D. Sannino, A. Baldacci, Catal. Today 29 (1996) 161.
[17] C. Martin, M.J. Martin, V. Rives, Stud. Surf. Sci. Catal. 72 (1992) 415.
[18] J. Loewenschuss, M. Shamir Ardon, Inorg. Chem. 15 (1976) 238.
[19] C.P. Cheng, G.L. Schrader, J. Catal. 60 (1979) 276.
[20] A. Duan, G. Wan, Z. Zhao, C. Xu, Y. Zheng, Y. Zhang, T. Dou, X. Bao, K. Chung, Catal. Today 119 (2007) 13.
[21] M.S. Rana, S.K. Maity, J. Ancheyta, G. Murali Dhar, T.S.R. Prasada Rao, Appl. Catal. A: Gen. 268 (2004) 89.
[22] S. Braun, L.G. Appel, V.L. Camorim, M. Schmal, J. Phys. Chem. B 104 (2000) 28.
[23] M. Cheng, F. Kumata, T. Saito, T. Komatsu, T. Yashima, Appl. Catal. A: Gen. 183 (1999) 199.
[24] R. Gòmez, T. Lòpez, E. Ortis-Islas, J. Navarrete, E. Sànchez, F. Tzompanztzi, X. Bokhimi, J. Mol. Catal. A: Chem. 193 (2003) 217.
[25] S. Malato, J. Blanco, M.I. Maldonado, P. Fernandez-Ibanez, A. Campos, Appl. Catal. B: Environ. 28 (2000) 163.
[26] I.E. Wachs, G. Deo, D.S. Kim, M.A. Vuurman, H. Hu, in: Proceedings of 10th International Congress on Catalysis, Budapest, Hungary, (1992), p. 543.